

pubs.acs.org/acscatalysis Research Article

High-Temperature Pretreatment Effect on Co/SiO₂ Active Sites and Ethane Dehydrogenation

Kewei Yu, Sanjana Srinivas, Cong Wang, Weiqi Chen, Lu Ma, Steven N. Ehrlich, Nebojsa Marinkovic, Pawan Kumar, Eric A. Stach, Stavros Caratzoulas, Weiqing Zheng,* and Dionisios G. Vlachos*



Cite This: ACS Catal. 2022, 12, 11749-11760



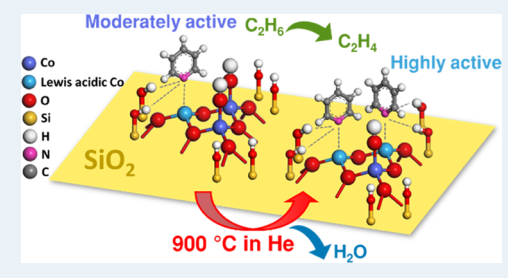
ACCESS I

Metrics & More

Article Recommendations

s Supporting Information

ABSTRACT: We report the synthesis, optimization, and characterization of Co/SiO₂ for ethane nonoxidative dehydrogenation. Co/SiO₂ is synthesized via strong electrostatic adsorption using the widely available $Co(NO_3)_2$ as the precursor. We demonstrate that high-temperature pretreatment (900 °C) in an inert atmosphere can significantly enhance the initial activity of the Co/SiO₂ catalyst. X-ray absorption near-edge spectroscopy (XANES), temperature-programmed reduction (TPR), and high-angle annular dark-field scanning transmission electron microscopy (HAADF-STEM) suggest that highly dispersed Co(II) clusters are more active than Co^0 or CoO_x nanoparticles. Fourier transform infrared (FTIR) and isopropanol (IPA) temperature-programmed desorption and density func-



tional theory (DFT) calculations suggest that high-temperature treatment significantly increases the density of active Lewis acid sites, possibly via surface dehydroxylation of the catalyst.

KEYWORDS: ethylene, Lewis acid, earth-abundant catalysts, shale gas, dehydrogenation

1. INTRODUCTION

Olefins are essential platform intermediates leading to polymers, ethylene and propylene oxide, acrolein, and many other chemicals. Small olefins, such as ethylene and propylene, have been produced chiefly from naphtha and natural gas liquids (NGLs) via steam cracking or fluid catalytic cracking. However, the high energy consumption, low selectivity, and dwindling petroleum reserves significantly challenge these processes. The recent shale gas revolution makes the catalytic dehydrogenation of light alkanes a viable solution for small olefin production. Pt-Sn/Al₂O₃ and CrO_x/Al₂O₃ are commercial dehydrogenation catalysts. Yet, the high material cost in the case of Pt, toxicity in the case of Cr, and severe deactivation are major hurdles driving the development of new catalysts.

In recent years, earth-abundant metals, such as Fe,⁵ Zn,^{6,7} Ni,⁸ Cr,^{9,10} and Co^{11–15} with high dispersion on oxide supports, have been explored as active and selective C–H bond activation catalysts. Among these catalysts, highly dispersed cobalt species on metal oxides exhibit promising activity and selectivity to olefins.¹¹ These catalysts have been synthesized using the strong electrostatic adsorption^{15,16} (SEA), surface organometallic chemistry^{13,14} (SOMC), atomic layer deposition¹⁷ (ALD), and flame spray pyrolysis^{11,12} (FSP). Some of these methods are complex or expensive, e.g., SEA using a cobalt hexa-ammine precursor. In addition, Co/SiO₂ catalysts are not as active compared to traditional Pt-and Cr-based catalysts. More facile and effective synthesis

producing highly dispersed Co catalysts with enhanced dehydrogenation performance would have been welcome.

Highly dispersed Co(II) single atoms are generally believed to be the active species for alkane dehydrogenation, but prior work is not conclusive. For example, Hu et al. suggested that Co single atoms bonded to the oxygen atoms of the SiO2 are the active sites, 15 and Estes et al. used SOMC methods to synthesize well-defined Co/SiO₂ and came to the same conclusion that isolated Co(II) is active. 13,14,18 In addition, Huang et al. compared their ALD-made Co/SiO2 with impregnated Co/SiO₂ and concluded that isolated cobalt species are active, whereas bulk cobalt oxide clusters are not. 17 On the other hand, Koirala et al. argued that isolated Co²⁺ in a surface cobalt silicate-like phase is the active species, 12 and Hu et al. also came to a similar finding that the tetrahedral Co²⁺ in the cobalt aluminate spinel (CoAl₂O₄) phase acts as the active site. 19 Recently, Lee et al. suggested that the subnanometer Co₄O₄ cluster can also dehydrogenate cyclohexane, ²⁰ and Wang et al. suggested that isolated CoO sites are active.²¹ In other studies, ultrasmall metallic Co was found to be active, 22,23 although metallic Co nanoparticles are generally believed to catalyze side reactions such as cracking and coke

Received: July 1, 2022
Revised: August 31, 2022
Published: September 13, 2022





formation. 24–27 In recent years, zeolite-supported Co-based dehydrogenation catalysts are also emerging for their enhanced stability and activity. 24,28–31 Due to the small size of these active Co species and the intimate contact with the support, the sites' local coordination and chemical environment can differ among studies and influence their properties. Additionally, the Co sites can undergo dynamic changes in response to the gaseous atmosphere and temperature. More detailed studies are needed to understand these effects.

In this work, we apply a facile 2-pot SEA method, using $Co(NO_3)_2$ as the cobalt source, to synthesize highly active and selective Co/SiO₂ catalysts for ethane (nonoxidative) dehydrogenation (EDH). X-ray absorption near-edge spectroscopy (XANES), temperature-programmed reduction (TPR), and high-angle annular dark-field scanning transmission electron microscopy (HAADF-STEM) suggest that Co(II) single atoms and some ultrasmall clusters are the most active species. The effect of cobalt loading and catalyst pretreatment on performance is investigated. We discovered that a simple heating pretreatment in an inert atmosphere at 900 °C leads to a 4X activity boost. Using Fourier transform infrared (FTIR) and temperature-programmed desorption (TPD), we propose that site restructuring, caused by surface dehydroxylation, drives the improved dehydrogenation activity. Density functional theory (DFT) calculations confirm that high temperatures can promote dehydroxylation of cobalt sites, creating undercoordinated sites with higher Lewis acidity. Importantly, the catalyst can be regenerated by calcination followed by thermal treatment. We shed light on the dynamics of the Co(II) active site and the design of highly active Co/SiO₂ catalysts.

2. EXPERIMENTAL METHODS

2.1. Catalyst Synthesis and Pretreatment. For the SEA- Co/SiO_2 , 5 g of silica (FUJI SILYSIA G6, 3 μm) was suspended in 100 mL of aqueous solution at a pH of 11 adjusted using an ammonium hydroxide solution. 15,32 Co- $(NO_3)_2 \cdot 6H_2O$ (Sigma-Aldrich, purity $\geq 98.0\%$) and NH_4Cl (Fisher Chemical, purity ≥99.0%) were fully dissolved in 25 mL of diluted ammonia solution (Fisher Chemical). The cobalt complex solution was slowly injected into the silica suspension with a syringe, forming a bright blue suspension of Co/SiO₂. The cobalt loading was 0.05, 0.1, 0.2, 0.4, 0.6, and 0.8 mmol Co/g-SiO₂. After aging, the suspension was filtered and washed with deionized (DI) water 5 times. The solid paste was then dried in an air oven at 120 °C for 18 h, pelletized, broken, and sieved to 40-60 mesh (250-400 μ m); it is hereafter denoted generically as EA-Co/SiO₂ or specifically as $EA-xCo/SiO_2$, where x denotes the mmols of Co per g of SiO₂. The EA-Co/SiO₂ was annealed in helium at 700 °C (denoted as EA-Co/SiO₂-fresh). The annealed EA-Co/SiO₂-fresh was then annealed again in He at 900 °C in the reactor prior to the reaction (denoted as EA-Co/SiO₂-pretreated). Co/SiO₂ was also synthesized through the incipient wetness impregnation (IWI) method with an aqueous solution of cobalt(II) nitrate hexahydrate. The silica support was calcined at 700 °C for 1 h prior to impregnation. After impregnation and drying at 120 °C overnight, the IWI-Co/SiO₂ catalyst was calcined in air at 700 °C for 3 h.

2.2. Catalyst Characterization. 2.2.1. X-ray Characterizations. Wavelength dispersive X-ray fluorescence (WDXRF) was conducted on a Rigaku Supermini 200 WDXRF with a 50 kV, 200 W Pd-anode X-ray tube under a helium atmosphere. X-ray diffraction (XRD) was performed on an X-ray powder

diffractometer (Bruker D8) equipped with a monochromatic Cu K α source over a 2θ range of $10-80^\circ$ with a step size of 0.05° and 1 s/step. Cobalt K edge (7709.0 eV) X-ray absorption spectroscopy (XAS) was performed at the beamline 7-BM (QAS) in the National Synchrotron Light Source II (NSLS II) at the Brookhaven National Laboratory. Spectra were collected in a transmission mode. XAS data was processed with the Athena software (0.9.26) following standard procedures. ³³

2.2.2. FTIR Spectroscopies. In situ Fourier transform infrared spectroscopy (FTIR) chemisorption was conducted in a custom-made vacuum cell. The catalyst was first pressed into a thin pellet and degassed in the infrared (IR) cell in vacuum at 300 °C for 1 h. After degassing, the cell was ramped down to 150 °C for chemisorption and spectra acquisition. An excessive amount of pyridine/acetonitrile- D_3 was added to the cell to saturate the sample, and then a vacuum was applied to remove the excess gas phase and physisorbed molecules. Spectra were collected with a Thermo Fisher Scientific Nicolet 8700 FTIR spectrometer. Semiquantification of chemisorbed molecules on different samples was conducted after normalizing the molecular adsorption signal with the band intensities from the silica support.

2.2.3. Electron Microscopy. The bright-field transmission electron microscopy (TEM) images were obtained with a JEOL (JEM-2010F) transmission electron microscope equipped with a field emission gun emitter at 200 kV. Dark-field scanning transmission electron microscopy was performed with a JEOL NEOARM operating at 200 kV. The samples were diluted in isopropanol (IPA) and deposited on a lacey carbon film on copper grids provided by the Electron Microscopy Sciences.

2.2.4. Temperature-Programmed Studies. In temperature-programmed reduction (TPR) experiments, after pretreating the samples at 200 °C in helium (Keen Compressed Gas, ultrahigh purity, 99.999%) for 1 h, Co/SiO_2 (100 mg) was reduced in a 5% H_2 (Matheson, ultrahigh purity, 99.999%)/He (total 60 sccm) stream. The reduction temperature was increased from 200 to 1000 °C at a heating rate of 10 K/min. The effluent hydrogen gas was analyzed by a quadrupole mass spectrometer (QMS) (Pfeiffer Vacuum Omnistar GSD 301C). The temperature ramp was started after a stable H_2 baseline was observed. Helium (m/z=4) was used as the internal reference to obtain a stable hydrogen baseline. TPR quantification was enabled using CuO as a standard sample to calibrate the QMS signal for hydrogen consumption.

In the IPA temperature-programmed desorption (IPA-TPD) experiment, 100 mg of catalyst was loaded in the reactor, pretreated in a flowing He at 625 °C, saturated with IPA, and then purged with helium at 80 °C for 2 h to remove excessive IPA. The catalyst was then heated to 800 °C with a ramp rate of 10 K/min. The desorbed species were analyzed using the QMS for hydrogen (m/z=2), helium (m/z=4), acetone (m/z=43), propylene (m/z=41), carbon dioxide (m/z=44), and water (m/z=18).

2.3. Catalyst Performance Tests. Dehydrogenation reactions were conducted in an atmospheric pressure continuous flow tubular quartz reactor of a 7 mm inner diameter. For activity and regeneration tests, 100 mg of pelletized catalyst was loaded into the reactor. The bed was fixed by quartz wool and quartz pellets above and below the bed. The flow rates of C_2H_6 (Matheson, purity $\geq 99.5\%$), H_2 , and He were regulated by calibrated thermal mass flow

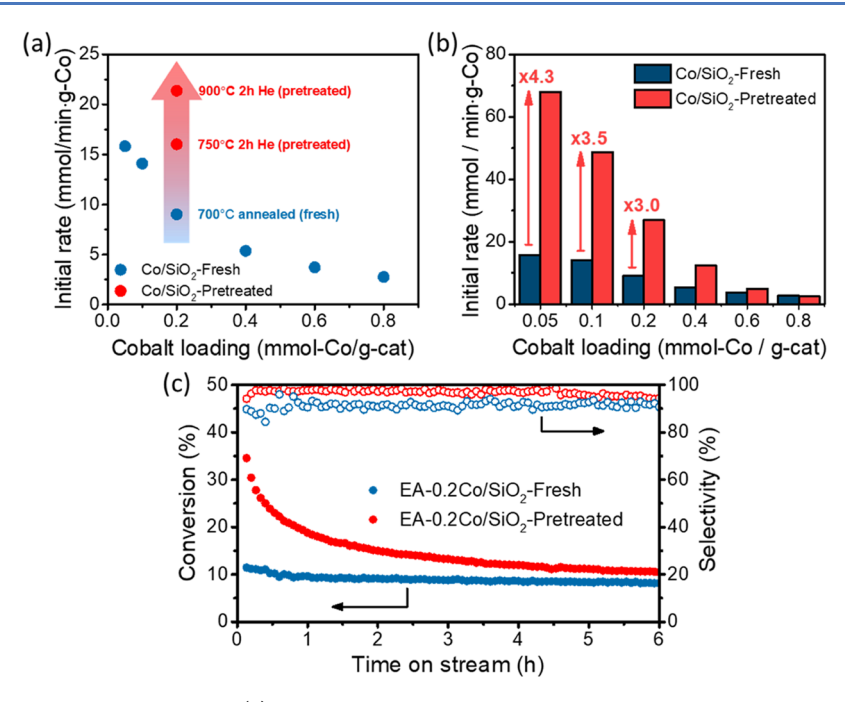


Figure 1. Ethane dehydrogenation reactivity results. (a) Activity of EA-0.2Co/SiO₂ and IWI-Co/SiO₂ and the effect of annealing temperature on the initial rate of EA-0.2Co/SiO₂-fresh (rate calculated from the C_2H_6 conversion; the selectivity of IWI-Co/SiO₂ is close to 0; see the Supporting Information). (b) Initial rates of EA-xCo/SiO₂ (fresh and pretreated) of various cobalt loadings per gram of cobalt. (c) Time on stream reactivity test of EA-0.2Co/SiO₂-fresh and EA-0.2Co/SiO₂-pretreated. Pretreatment condition: 900 °C in 80 sccm He for 1 h; reaction conditions: 4% C_2H_6 He, 60 sccm total, 625 °C, 100 mg of catalyst. WHSV = 1.77 h⁻¹ (C_2H_6 based); equilibrium conversion: 65%; gas-phase conversion at 625 °C (empty reactor): 0.51%.

controllers (MKS Instruments). Typical conditions in a reaction were 4% C₂H₄ in He, 60 SCCM total flow rate, 625 °C. The effluent gas compositions were measured using a MicroGC (990 MicroGC, Agilent) at 4 min intervals.

The conversion and selectivity were calculated based on the differences in inlet and outlet gas compositions. As shown in eqs 1 and 2, $[C_2H_6]_0$ represents the inlet ethane concentration, while terms without the subscript represent the outlet concentrations. The change in the volumetric flow rate is neglected due to the high dilution.

$$X_{C_2H_6} = \frac{[C_2H_6]_0 - [C_2H_6]}{[C_2H_6]_0} \times 100\%$$
 (1)

$$S_{C_2H_4} = \frac{[C_2H_4]_0}{[C_2H_6]_0 - [C_2H_6]} \times 100\%$$
 (2)

Fresh catalysts were used for each data point to minimize the effects from catalyst deactivation, except for the deactivation and regeneration studies. The initial rates were collected 4 min after starting the reactant flow when a stable concentration of the reactants was established. The carbon balance remained above 98% in all experiments.

2.4. Computational Methods. All electronic structure calculations were performed in Gaussian 09, Revision D.01. The Si, O, and H atoms were modeled at the B3LYP³⁵/def2SVP theory level, and the Co atom was modeled at the B3LYP/def2TZVP theory level. An empirical dispersion correction by Grimme³⁶ was added to the DFT energies.

3. RESULTS AND DISCUSSION

3.1. Effect of Cobalt Loading and Pretreatment on the Activity of EA-Co/SiO₂. EDH over EA-Co/SiO₂ catalysts with Co loading ranging from 0.05 to 0.8 mmol Co/g-SiO₂ at

625 °C shows high activity and selectivity to ethylene (Figures 1 andS1). Figure 1c shows time on stream data (TOS), highlighting the high selectivity and high conversion, approaching thermodynamic equilibrium (see the caption of Figure 1 for details). In Figure 1a, the initial rate (over the total Co loading) increases with lowering the cobalt loading, suggesting that the dispersion and/or morphology of Co plays an important role. In contrast, the freshly calcined IWI-0.4Co/SiO₂ shows little EDH activity (Figure S2). Highly dispersed Co species are catalytically essential, consistent with previous studies. ^{12,15,17,18,37}

Interestingly, thermal pretreatment of the fresh catalyst at higher temperatures (>700 °C) in an inert gas flow, such as He or N2, increases the initial rate significantly. Higher temperature and longer treatment time lead to higher activity (Figures 1a and S3). As highlighted in Figure 1a, a 900 °C He pretreatment increases the rate 3× for EA-0.2Co/SiO₂-fresh, without sacrificing selectivity. Most of the benefit from annealing at 900 °C occurs within 1 h, and this is used hereafter. The activity of the pretreated catalyst is among the highest in similar Co-based dehydrogenation catalyst studies (Table S1). The effect of pretreatment on the initial reaction rates is summarized in Figure 1b, with per gram catalyst-based rate presented in Figure S1. The initial ethane rate is less enhanced with increasing Co loading, likely due to sintering at high Co loadings and loss of surface area (Table S2). To understand the nature of the active site and the effect of hightemperature pretreatment, we conduct catalyst characterization and computation in the following sections.

3.2. Structural and Chemical Properties of EA-Co/SiO₂. 3.2.1. Structural Characterization of EA-Co/SiO₂. Structural and chemical characterizations are conducted to identify the EA-Co/SiO₂ species and reveal the high-temper-

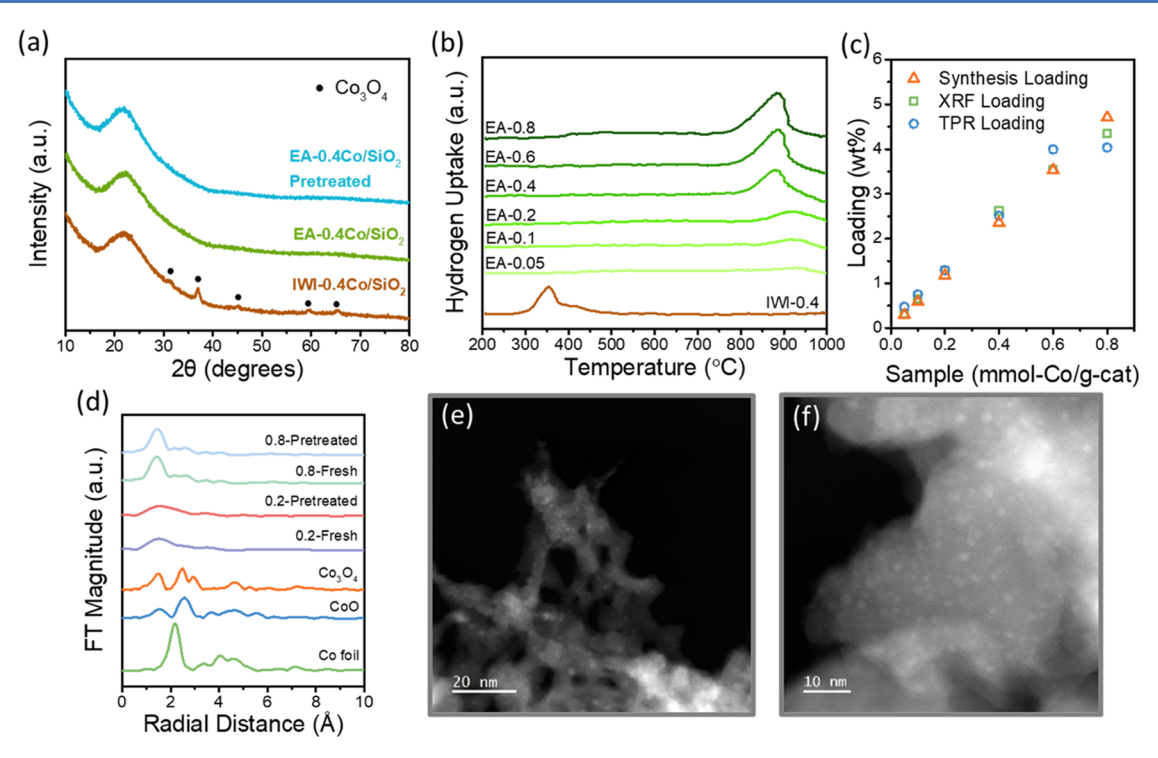


Figure 2. Structural characterizations of Co/SiO_2 catalysts. (a) XRD pattern of IWI-0.4 Co/SiO_2 , EA-0.4 Co/SiO_2 -fresh, and EA-0.4 Co/SiO_2 -pretreated. (b) TPR of EA- Co/SiO_2 of all loadings and IWI-0.4 Co/SiO_2 . (c) Cobalt loadings from XRF, TPR (assuming Co/O = 1:1), and nominal values in the synthesis (amount of $Co(NO_3)_2$ used). (d) Fourier-transformed k2-weighted magnitude of EXAFS data vs radial distance of EA- Co/SiO_2 -fresh and pretreated with 0.2 and 0.8 loadings and references (Co_3O_4 , CoO, and cobalt foil). (e, f) HAADF-STEM images of EA- Co/SiO_2 -fresh.

ature pretreatment effect. It has been demonstrated that the SEA method can improve the dispersion of supported metal nanoparticles. 32,38 As shown in Figure 2a, the IWI method leads to $\rm Co_3O_4$ nanoparticles identified by XRD. In contrast, the EA-Co/SiO $_2$ catalyst does not show any diffraction pattern associated with cobalt, even after high-temperature pretreatment, indicating its high dispersion.

To understand the metal-support interaction, we conducted TPR measurements (Figure 2b). The IWI-Co/SiO₂ sample has a major reduction peak around 350 °C associated with the reduction of Co₃O₄ clusters.³⁹ The TPR profiles of the SEA-Co/SiO2 exhibit vastly different behavior, with a reduction above 900 °C (EA-0.05Co/SiO₂) and slightly lower temperatures (>800 °C) with increasing Co loading. This indicates that the cobalt species in EA-Co/SiO₂ are already reduced to a good extent and strongly interact with the silica support, making it difficult to reduce. The H₂/Co ratio, quantified from the TPR profiles, is close to 1:1 in all samples (Figure 2c), suggesting a Co²⁺. The nominal cobalt loading and those from XRF and TPR (Figure 2c) are in good agreement. Using Fourier-transformed EXAFS spectra of the catalysts and standards (Figure 2d), we further confirm the high dispersion of cobalt species: metallic Co, CoO, and Co₃O₄ standards all show significant Co-Co scatterings, whereas the EA-Co/SiO₂ samples only show Co-O scatterings at less than 2 Å, indicating that Co atoms mainly coordinate with the O atoms of the support and are spatially segregated with each other. In addition, the lack of features at long radial distances indicates the long-range disorder of the cobalt species. EXAFS fitting gives an average Co-O bond length of 1.9855 Å for the EA-0.8Co/SiO₂ samples and a coordination number of 4.86 \pm 1.05 and 4.60 \pm 2.25 for the fresh and pretreated EA-0.8Co/

 ${
m SiO_2}$ samples, respectively. A coordination number slightly greater than 4 may indicate the coexistence of Co oxide clusters in the high-loading samples.

Ultraviolet—visible (UV—vis) spectra of EA-Co/SiO₂-fresh across all loadings (Figure S4) show characteristic bands at three locations, 520, 590, and 650 nm, generated by the d—d transition of the Co(II) atoms in the tetrahedral coordination. The band intensity grows with increasing cobalt loading. The pretreated samples show no significant change in band locations (Figure S5). In contrast, the IWI-Co/SiO₂ catalyst only shows band characteristics of Co₃O₄¹⁷ (Figure S4). HAADF-STEM images of the fresh (Figure 2e,f) and pretreated (Figure S6) EA-0.2Co/SiO₂ catalysts show highly dispersed CoO_x clusters.

In summary, the EA-Co/SiO $_2$ contains mostly highly dispersed Co species in the 2^+ oxidation state, tetrahedrally coordinated, likely in single atoms, clusters, or oligomers strongly bonded to the ${\rm SiO}_2$ support. The properties of these species are vastly different from those of cobalt oxide clusters of the IWI sample. However, the subtleness in the high-temperature pretreatment effect makes these bulk techniques ineffective to tell the differences. We resort to molecular probes below to understand the catalyst change during pretreatment.

3.2.2. Probing the Lewis Acid Sites with Pyridine and Acetonitrile- D_3 . Lewis acidic tetrahedral Co(II) and basic O pairs are believed to be the active sites for alkane dehydrogenation. The reaction mechanism has been proposed to include ethane C-H bond activation and adsorption on the Lewis acidic Co(II) site. The hydrogen atom is then subtracted by the O atom in the vicinity of the Co atom, and the ethyl group bonds to the Co(II) atom. Next, a β -H is

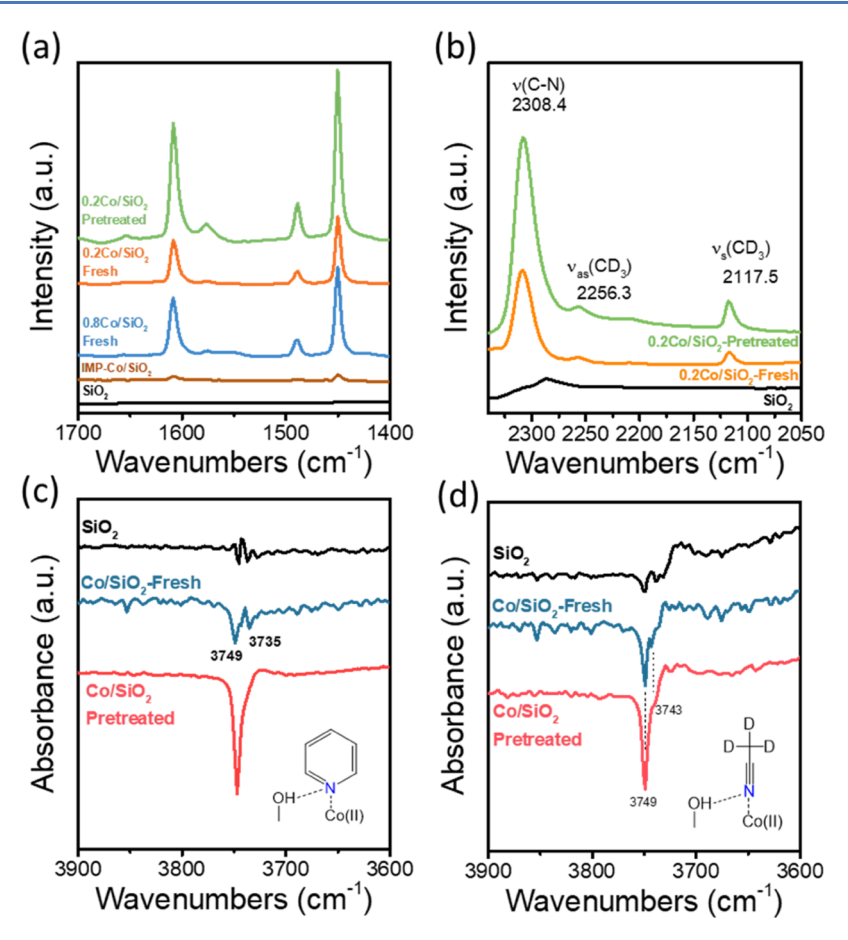


Figure 3. Differential FTIR absorption spectra. (a) Pyridine chemisorption on EA-0.2Co/SiO₂-fresh, EA-0.2Co/SiO₂-pretreated, EA-0.8Co/SiO₂-fresh, IWI-0.4Co/SiO₂, and SiO₂ collected at 150 °C after evacuation. (b) Acetonitrile-D₃ chemisorption on EA-0.2Co/SiO₂-fresh, EA-0.2Co/SiO₂-pretreated, and SiO₂ support collected at 30 °C after evacuation. (c) OH stretching region of SiO₂, Co/SiO₂-fresh, and Co/SiO₂-pretreated after pyridine adsorption and evacuation for 10 min at 150 °C. (d) OH stretching region of SiO₂, Co/SiO₂-fresh, and Co/SiO₂-pretreated after acetonitrile-D₃ adsorption and evacuation for 10 min at 30 °C. All spectra normalized with bands from 1800 to 2200 cm⁻¹ of SiO₂.

eliminated by Co. The remaining vinyl group desorbs as ethylene. Finally, the subtracted hydrogen atoms recombine and desorb as molecular H₂. Co–O acts as a Lewis acid–base pair to activate the C–H bond and accept the ethyl group and proton, respectively.

We used pyridine as a probe molecule for in situ FTIR measurements of the acid catalyst properties. In Figure 3a, EA-Co/SiO₂ samples show bands at 1612, 1492, and 1451 cm⁻¹, characteristic of Lewis acid centers, without the 1540 cm⁻¹ feature of Brønsted acid sites. ⁴⁴ The pure SiO₂ support did not show any pyridine adsorption. There is hardly any chemisorbed pyridine on the IWI-Co/SiO₂ catalyst, suggesting that the Lewis acid centers are directly associated with the highly dispersed Co species.

CD₃CN, another commonly used base molecule, can probe surface acidity predominately of Lewis acid sites by interacting with them through its nitrogen lone pair electron donation. The shift from the liquid-phase C–N vibrational frequency (2265 cm⁻¹) can distinguish Lewis from Brønsted acids and is representative of the acid strength. In Figure 3b, the main absorption band at 2308.4 cm⁻¹ is assigned to the C–N stretching mode of chemisorbed CD₃CN. Less intensive bands at 2256 and 2117 cm⁻¹ are assigned to the fundamental asymmetric and symmetric C–D stretches, respectively. The main band has a Δv (CN) of 46.4 cm⁻¹ in the region of Lewis coordinated nitrile species (40–60 cm⁻¹). Nitrile species

interacting with Brønsted acid sites $(20-30~\text{cm}^{-1})$ are absent, ⁴⁷ consistent with the pyridine FTIR results.

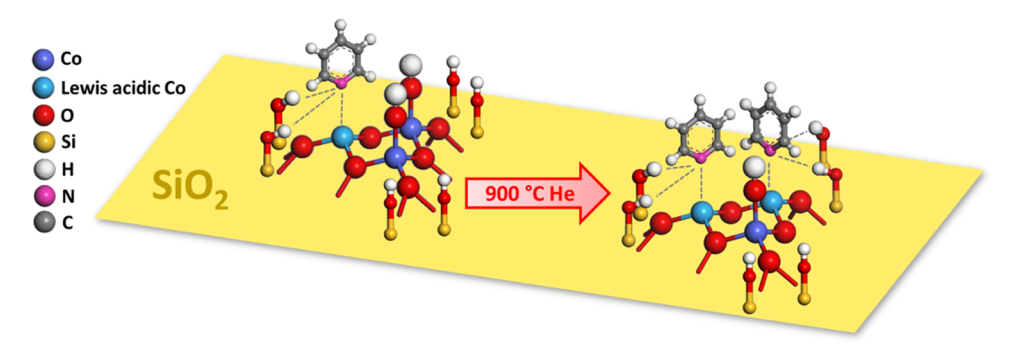
The most intense band for pyridine at $1451~{\rm cm}^{-1}$ is integrated as a semiquantitative metric of Lewis acidic site density and correlated with the initial rate. A good correlation is established (Table 1). After high-temperature pretreatment, the reactivity enhancement of EA-0.2Co/SiO₂ (a representative sample) scales well with the Lewis acid site density. The pyridine adsorption area also scales well with reactivity for EA-0.8Co/SiO₂-fresh (4× Co loading compared to 0.2Co/SiO_2). Like the pyridine data, an ~3× increase in the main band area for the C–N stretching mode of the adsorbed

Table 1. Initial Rates, Pyridine Chemisorption FTIR Areas, Acetonitrile- D_3 Chemisorption FTIR Areas, and IPA-TPD H_2 Desorption Areas of EA-Co/SiO₂ Samples^a

sample	initial rate (mmol/min·g-Cat)	normalized pyridine area (au)	normalized acetonitrile- D_3 area (au)	normalized H ₂ desorption area (a.u.)
0.2-fresh	0.11	1	1	1
0.2- pretreated	0.31	2.4	2.7	3.9
0.8-fresh	0.12	1.1		1.04

 a The bands at 1451 cm $^{-1}$ for adsorbed pyridine and 2308 cm $^{-1}$ for CD $_{3}$ CN are used for semiquantification.

Scheme 1. Schematic of the Proposed Structural Evolution of Co(II) Site before and after High-Temperature Pretreatment of EA-Co/SiO₂



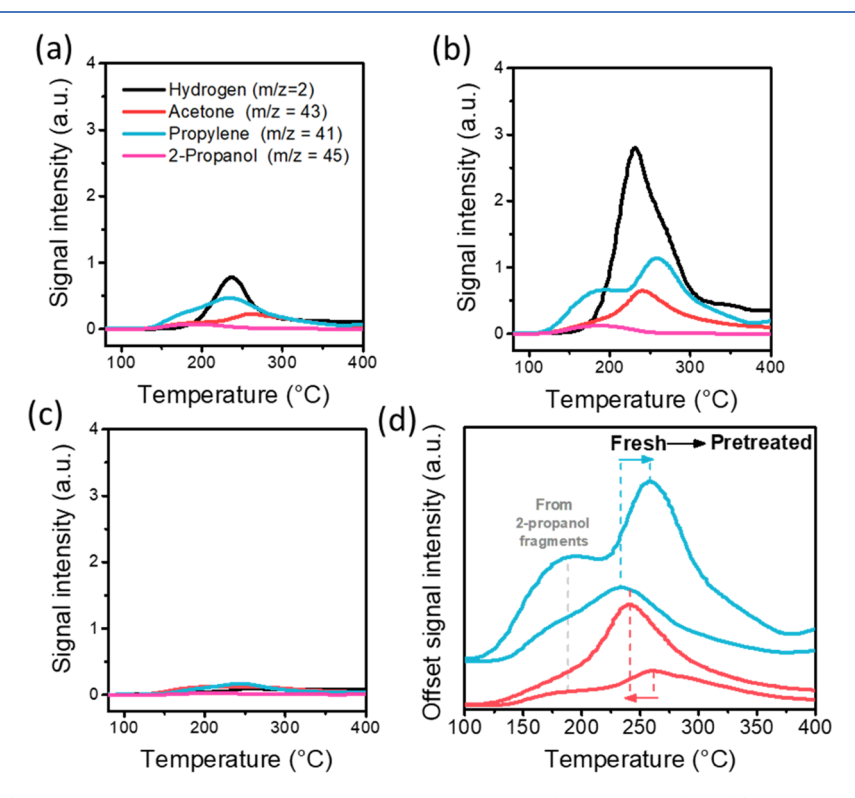


Figure 4. Isopropanol (IPA) temperature-programmed desorption-mass spectrometry (IPA-TPD-MS) of (a) EA-0.2Co/SiO₂-fresh, (b) EA-0.2Co/SiO₂-fresh and (c) IWI-0.2Co/SiO₂. (d) Propylene (m/z=41) and acetone (m/z=43) for fresh and pretreated catalysts. Samples are first degassed in He at 625 °C, then saturated with IPA at room temperature, purged with He again at 80 °C for 1 h to remove the weakly adsorbed IPA, and ramped up at 10 °C/min for TPD. Signals are normalized by He signal (m/z=4). Propylene (m/z=41) and acetone (m/z=43) signals are affected by the initial desorption of physisorbed IPA at ~190 °C.

CD₃CN is observed after pretreating the EA-0.2Co/SiO₂ catalyst (Table 1).

The adsorbed basic molecules on Co sites can also influence the neighboring silanol groups. As shown in Figure 3c,d, upon pyridine and acetonitrile- D_3 adsorption on EA-0.2Co/SiO₂, two negative bands appear around 3740 cm⁻¹, which correspond to the isolated Si–OH groups and weakly hydrogen-bonded Si–OH groups. These bands barely exist during the adsorption of pyridine and CD₃CN on pure SiO₂ (Figure 3c,d, black lines), indicating that the probes are not adsorbed directly by the Si–OH groups, causing the negative bands. Therefore, the negative bands form most likely from the interaction of the adsorbed probe molecules with the neighboring silanol protons to the Co site, as illustrated in Scheme 1. It is likely that the Co(II) sites are surrounded by the proximal Si–OH species and strongly interact with them.

After high-temperature pretreatment, the intensity of the negative -OH band significantly increases and scales with the amount of the adsorbed probe molecule, suggesting that more Co(II) species form. Overall, the semiquantitative chemisorption results of pyridine and acetonitrile- D_3 and the influence of the adsorbates on the surface silanol groups indicate a strong correlation between Lewis acid site density and EDH activity. 3.2.3. Probing Dehydrogenation Sites Using IPA-TPD-MS. To further confirm the increase in dehydrogenation site

To further confirm the increase in dehydrogenation site density, IPA-TPD-MS is applied, as IPA can undergo dehydration and dehydrogenation reactions on Lewis acid centers on metal oxides. S1,52 Upon feeding IPA, there is an immediate color change of the catalyst from light blue to purple, indicating that the adsorption of IPA on the cobalt sites changes their coordination environment. This phenomenon was also observed in prior studies. After IPA saturation at

Scheme 2. Mechanism for IPA Dehydrogenation and Dehydration on Lewis Acidic Co(II) Sites^a

^aType I: dehydration through a concerted E2 mechanism. Type II: dehydrogenation over a Co-O pair.

room temperature followed by 1 h purging in helium at 80 °C, dehydrogenation and dehydration products were observed as the temperature increased for EA-Co/SiO₂ samples (Figure 4a,b). In contrast, over IWI-0.2Co/SiO₂, little reaction occurs (Figure 4c). The water signal (m/z=18) is not shown because it desorbs over a wide temperature range. The weakly adsorbed IPA desorbs unreacted around 190 °C, and the shoulder peak of propylene at the identical position is due to the fragment of IPA.

The strong H_2 desorption between 200 and 300 °C, accompanied by the acetone signal from the dehydrogenation reaction, demonstrates that the high-temperature pretreatment significantly enhances the H2 and acetone signals up to 3× compared to the fresh EA-0.2Co/SiO₂ (Figure 4a,b), consistent with the reactivity and pyridine FTIR results. As shown in Figure S7, increasing Co loading to 0.8 mmol does not significantly increase the H2 desorption amount due to the aggregation of highly dispersed Co species. After hightemperature pretreatment, the EA-0.8Co/SiO₂ sample shows only a slight decrease in the H2 desorption amount suggesting the sintering of Co. This result aligns well with FTIR and reactivity data. Therefore, we believe that ethane and IPA may share a similar dehydrogenation mechanism, as illustrated in Scheme 2 (dehydrogenation pathway), and IPA dehydrogenation may be a reasonable proxy chemistry for EDH while also providing a competitive dehydration path.

The dehydration product, propylene (m/z = 41), appears above 200 °C, and there is also a minor increase in the desorption amount after pretreatment over EA-0.2Co/SiO₂. Lewis acid sites of metal oxides are generally active in alcohol dehydration.⁵² The increase in dehydrogenation and dehydration products indicates that the total Lewis acid site density in EA-0.2Co/SiO₂ increases with high-temperature pretreatment. Although both dehydrogenation and dehydration reactions can occur on Lewis acid sites, the fact that two different reactions occur on Co/SiO₂ suggests that there may be different local coordination environments of Co sites anchored on amorphous SiO₂ with distinct catalytic properties.

More interestingly, as demonstrated in Figure 4d, high-temperature pretreatment shifts the IPA dehydrogenation from 260 to 241 °C and the dehydration from 233 to 259 °C, suggesting that the Lewis acid centers become more favorable for dehydrogenation. We propose that the local coordination of Co has a strong effect on the Lewis acid site center and the reaction pathway. As illustrated in Scheme 2, the main difference between the two pathways lies in whether the active site can activate the alcohol O–H bond: strong Lewis acid—

base pairs can subtract H from the OH group of IPA to form acetone; if not, the C-O bond of the adsorbed IPA molecule eventually breaks to evolve propylene. In summary, IPA-TPD-MS results suggest that the pretreatment may influence the Lewis acid—base strength of the active sites and, in turn, their dehydrogenation activity.

The acid-base property of an active site is highly related to its local coordination environment. Both coordination geometry and electronic effect from neighboring atoms can affect the acidity and, in turn, the catalytic performance. Zhao et al. have demonstrated that by replacing the Si atom proximal to the Co site with Zr, the dehydrogenation activity of the Co/ SiO₂ catalyst improved due to the change in oxygen donor ability and Co-O bond strength. 16 Estes et al. reported that the distorted Co is more Lewis acidic and catalytically active than the standard tetrahedral Co species. 14 In this work, the high-temperature pretreatment in an inert atmosphere likely changes the local coordination geometry of the Co site by surface restructuring. By monitoring the effluent gas during pretreatment, we observe continuous desorption of water at ~700 °C (Figure S8), and dehydroxylation continues even at 900 °C. Moreover, when exposing the pretreated catalyst to 1% H₂O/He before reaction at 625 °C, the reactivity of the catalyst is significantly reduced (demonstrated in Section 3.4). Therefore, the EA-Co/SiO₂ catalysts prepared by SEA form highly dispersed Co clusters and create highly active Co(II)based Lewis acid centers for dehydrogenation. High-temperature pretreatment leads to a deep dehydroxylation, especially at the Co(II) center and neighboring Si-OH, creating Co-O-Si bridges, which turns Co-O into a stronger Lewis acidbase pair and more active for dehydrogenation, as illustrated in Scheme 1. We propose that the degree of hydroxylation of the SiO₂ surface, especially at the Co-SiO₂ interface, may play an important role in the Co(II) site structure and, in turn, influence the dehydrogenation activity of the site.

3.3. Computational Evidence of Enhanced Lewis Acidity after Dehydroxylation. We hypothesize that the high-temperature treatment of the catalyst in an inert atmosphere results in the removal of -OH ligands of Co(II) as water, creating distorted tetrahedral or undercoordinated Co sites that are stronger Lewis acids.

To validate this hypothesis, we compute the binding energies of pyridine and deuterated acetonitrile on hydroxylated and dehydroxylated Co(II)/SiO_2 cluster models, which represent fresh and pretreated catalysts, respectively. We assume that dehydroxylation at high temperatures can result in the formation of Co-O-Si, Si-O-Si, or Co-O-Co

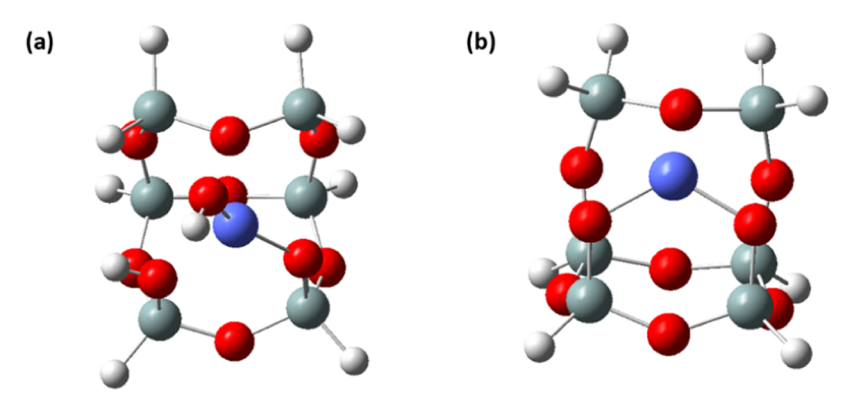


Figure 5. Cluster models (a) before (presence of Co–OH) and (b) after (Co–O–Si bridge formation) pretreatment. (Atom labeling: H, white; O, red; Si, green; Co, blue).

bridges. Each of these cases has been investigated by DFT calculations using mononuclear or dinuclear $Co(II)/SiO_2$ cluster models; the thermodynamic feasibility of dehydroxylation has also been assessed.

We investigated three outcomes of dehydroxylation induced by pretreatment.

Case 1: Formation of Co-O-Si Bridge. Figure 5 shows the active site before (Co-OH) and after pretreatment (Co-O-Si) and the change in the coordination of Co(II) from tetracoordinate to tri-coordinate. Table 2 shows the binding

Table 2. Binding Energies of Pyridine, Deuterated Acetonitrile, and Ethylene on the Fresh and Pretreated Catalysts: Co-O-Si Bridge Formation

site structures	pyridine binding energy (eV)	CD ₃ CN binding energy (eV)	$\begin{array}{c} C_2H_4 \\ \text{binding} \\ \text{energy (eV)} \end{array}$
fresh catalyst (Co-OH) (Co-O-Si bridge)	-1.07	-0.49	-0.36
pretreated catalyst (Co- O-Si) (Co-O-Si bridge)	-1.68	-1.24	-1.03
fresh catalyst (Si-OH) (Si-O-Si bridge)	-0.98	-0.60	-0.57
pretreated catalyst (Si-O-Si) (Si-O-Si bridge)	-1.56	-1.13	-0.93
fresh catalyst (Co-OH- Co) (Co-O-Co bridge)	-1.43	-0.85	-0.83
pretreated catalyst (Co– O–Co) (Co–O–Co bridge)	-2.21	-1.23	-0.92

energies of the two probe molecules on tetra-coordinate and tri-coordinate Co(II). The significantly larger binding energies at the tri-coordinate site clearly indicate stronger Lewis acidity post dehydroxylation. Both before and after dehydroxylation, the ground electronic state of the system is a quartet.

We also assessed the thermodynamics of the formation of the Co–O–Si bridge at different temperatures by calculating the free-energy change $\Delta G_{\rm dehydrox} = G_{\rm pretreated} + G_{\rm H_2O} - G_{\rm fresh}.$ At 900 K (reaction temperature), $\Delta G_{\rm dehydrox} = -0.03$ eV, whereas at 1173 K (pretreatment temperature), $\Delta G_{\rm dehydrox} = -0.35$ eV, indicating that dehydroxylation and bridge formation become increasingly favorable with temperature.

Case 2: Formation of Si–O–Si Bridge. Figure 6 shows the active site before and after pretreatment, where two silanols near the Co(II) species condense to form a Si–O–Si bridge. Table 2 shows the corresponding binding energies of the probe molecules, which reveal a stronger Lewis acidity of the undercoordinated Co(II) atoms. As in case 1, the ground electronic state of the system is a quartet both before and after binding of the probe molecules. Our calculations show that, at 900 K, the Si–O–Si bridge formation is thermodynamically unfavorable ($\Delta G_{\rm dehydrox} = 0.13$ eV) but becomes more favorable at 1173 K ($\Delta G_{\rm dehydrox} = -0.27$ eV). Case 3: Formation of a Co–O–Co bridge. Figure 7 shows

Case 3: Formation of a Co–O–Co bridge. Figure 7 shows two adjacent Co(II) sites, each with a OH ligand, in the fresh catalyst, and a dinuclear Co–O–Co site that forms upon water elimination. Once again, the stronger binding energies reported in Table 2 for the model representing the pretreated catalyst are consistent with our hypothesis that dehydroxylation results in greater Lewis acidity. The active sites in the pretreated catalyst show a more distorted tetrahedral structure when compared to the fresh catalyst, which could be responsible for the greater acidity. The free-energy change at 900 and 1173 K, $\Delta G_{\rm dehydrox}=0.35$ and 0.0 eV, respectively, indicates that the Co–O–Co bridge formation is less favorable than the formation of Co–O–Si or Si–O–Si bridges.

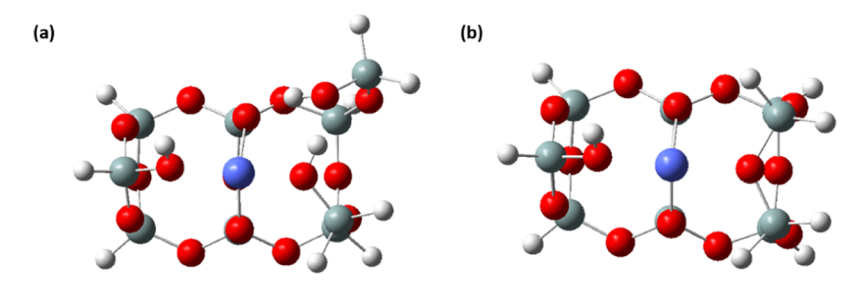


Figure 6. Cluster models (a) before (presence of Si-OH) and (b) after (Si-O-Si bridge formation) pretreatment. (Atom labeling: H, white; O, red; Si, green; Co, blue).

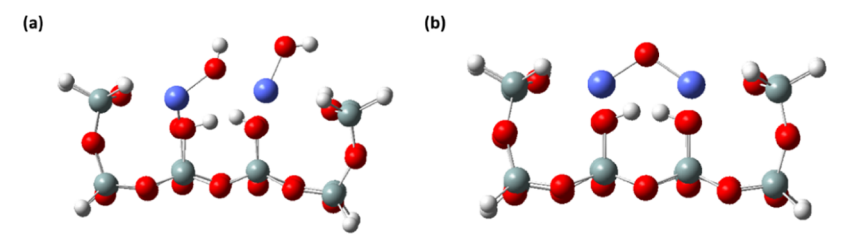


Figure 7. Cluster models (a) before (presence of Co-OH) and (b) after (Co-O-Co formation) pretreatment. (Atom labeling: H, white; O, red; Si, green; Co, blue).

While pretreatment increases the number of available Lewis acid sites, it could also enhance the rate of catalyst degradation via coking. The binding energy of ethylene can be used as a descriptor for coking. Table 2 shows that ethylene binds a lot more strongly on the pretreated catalyst than on the fresh catalyst, which is conducive to coke formation.

Thus, our calculations suggest that at high temperatures, multiple (M)—OH ligands of Co(II) can condense and result in undercoordinated active sites, which have higher Lewis acidity. We also see, both experimentally and computationally, that there is a tradeoff between activity and stability of the catalyst. While pretreatment enhances the initial rates, the higher Lewis acidity may lead to increased coking and faster catalyst degradation.

3.4. Stability and Regeneration of EA-Co/SiO₂. Although the initial rate of EDH can be significantly enhanced by high-temperature pretreatment, the activity drops by almost 70% in 6 h (Figure 1c). Coke formation is a possible reason for deactivation. The two Raman peaks (D-band around 1350 cm⁻¹ and G-band around 1600 cm⁻¹; Figure S9a) and graphitic layers on top of Co NPs (Figure S10c,d) confirm coke on spent catalysts. Calcination of the spent catalyst in air at 625 °C completely removes the coke, as confirmed by Raman (Figure S9a). While oxidizing the pretreated catalyst in air at 625 °C does not affect the high performance, as shown in Figure 8 (right-pointing triangles), coke removal by calcination

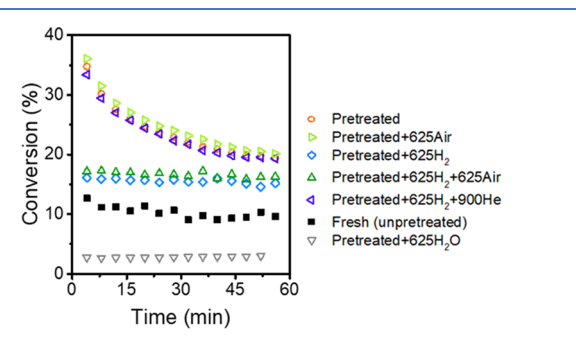


Figure 8. Activity of EA-0.2Co/SiO₂-pretreated catalyst exposed at reaction temperature in air (30 min), hydrogen (10% $\rm H_2$, 2 h), and water (1% $\rm H_2O$) prior to the reaction. The reactor is then purged with He for 1 h before catalytic testing (reaction condition: 625 °C, 4% $\rm C_2H_6$ in He, 60 SCCM).

does not recover the high reactivity (Figure 9a), indicating that coking is not the only reason for deactivation. Pyridine FTIR further confirmed that the Lewis acid site density is not fully recovered (Table S3). It is likely that the primary product $\rm H_2$ also affects the active sites of $\rm Co(II)$ species during the reaction. As shown in Figure 8 (diamonds), reducing the pretreated EA-Co/SiO₂ at 625 °C leads to a significant drop in ethane conversion from 35 to 16%, and the high reactivity is

recovered only by the high-temperature pretreatment at 900 °C rather than oxidation at 625 °C. XPS (Figure S9b) and TEM (Figure S10) characterization of the spent and reduced catalysts show that both samples contain some Co⁰ nanoparticles. Additionally, pyridine FTIR on the reduced Co/SiO₂ catalyst shows a decreased pyridine band area, which agrees well with the catalyst lower dehydrogenation activity (Table S3). All of these results suggest that H_2 has a negative effect on the Co/SiO₂ catalyst. In addition, we detect a trace amount of water (m/z = 18) during the reaction, which may stem from the partial reduction of Co(II) or impurities in the reactant gas. Due to the fact that the activity of the pretreated catalyst gradually approaches that of the unpretreated Co/SiO₂ in 6 h (Figure 1c), it is likely that H_2O rehydroxylates the Co(II) site, therefore converting the site to its original (before pretreatment) state. The detrimental effect of H₂O at the reaction temperature is also confirmed by the water pretreatment experiment in Figure 8 (downward triangles). On the other hand, the fresh catalyst shows remarkable stability, likely because the original Lewis acidic Co(II) sites are located in certain geometric locations of the amorphous SiO₂ support, making them less prone to hydroxylation and reduction.

Due to the reductive nature of the dehydrogenation reaction and difficulty in removing trace amounts of impurities in the reactant, it is challenging to prevent the catalyst from the negative effect of H₂. Catalyst regeneration is necessary. As illustrated in Figure 9a, two treatments are used to counteract these effects: air calcination at 625 °C for coke removal and He annealing at 900 °C for reversing the negative effect from H₂ and H₂O during the reaction, which are believed to share a similar mechanism as the high-temperature pretreatment of the fresh catalyst. Applying either one of them to the spent catalyst does not recover the catalyst activity. However, applying them sequentially recovers the catalyst activity almost fully. This further confirms the effectiveness of the high-temperature pretreatment strategy in improving the catalyst's activity. The catalyst is regenerable for multiple cycles (Figure 9b) and after 6 h time-on-stream (Figure 9c). The slight irreversible deactivation after each regeneration cycle could be related to the collapse of pore structures of silica support during the hightemperature treatment (Table S2).

4. CONCLUSIONS

EA-Co/SiO₂ for ethane dehydrogenation (EDH) was synthesized through strong electrostatic adsorption using $Co(NO_3)_2$ as a cobalt source. Through extensive characterizations using XRD, TPR, UV–vis, XPS, XANES, and HAADF-STEM, we find that the EA-Co/SiO₂ catalysts contain mainly highly dispersed Co(II) clusters. We demonstrate that high-temperature pretreatment in an inert atmosphere significantly improves the dehydrogenation activity. The highest specific

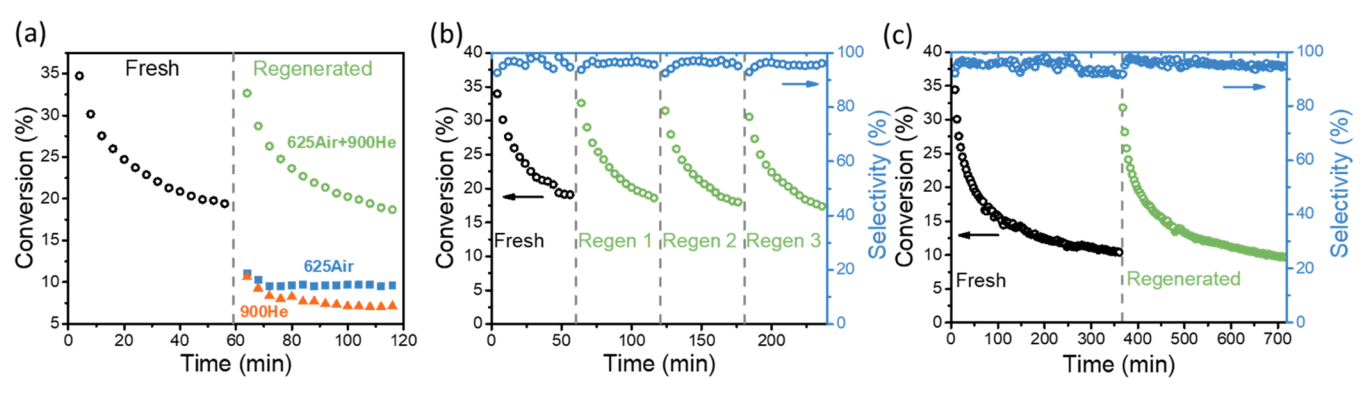


Figure 9. Regeneration of Co/SiO_2 : (a) regeneration with three different methods, (b) continuous regeneration for three cycles, and (c) regeneration after 6 h time-on-stream.

rate per gram of catalyst (0.31 mmol C₂H₆/min·g-cat) is reached at 0.2 mmol Co/g-cat loadings, and the highest specific rate per gram of cobalt (68.06 mmol C₂H₆/min·g-Co) is reached at 0.05 mmol Co/g-cat loading, which are among the highest in similar Co-based dehydrogenation catalyst studies. With pyridine, acetonitrile-D₃, and isopropanol as probe molecules in FTIR spectroscopy and temperatureprogrammed studies, a semiquantitative correlation was established between the surface Lewis acid site density and dehydrogenation activity. We propose that the cobalt sites undergo dehydroxylation during the high-temperature pretreatment, increasing the Lewis acid-base pair strength and therefore creating more active dehydrogenation sites. DFT calculations for three dehydroxylation scenarios confirm the necessity of high temperatures for the condensation of -OH groups, as well as the stronger Lewis acidity of the resulting undercoordinated Co sites. The increase in Lewis acidity agrees with our FTIR and IPA-TPD results and correlates with the higher dehydrogenation activity and faster deactivation (coking). Finally, we found that the pretreated catalyst can be regenerated by sequential postcalcination and high-temperature treatment.

This study may provide guidance for the future design of cobalt dehydrogenation catalysts. The local coordination and chemical environment are critical in the Co(II) site activity. By keeping the catalyst "dry" through the removal of H_2O and H_2 , one can maintain the high activity of the Co/SiO_2 catalyst. Owing to the recent advances and broad application of single-site metal oxide catalysts, high-temperature pretreatment can be a generic strategy for activity improvement and catalyst regeneration.

ASSOCIATED CONTENT

Supporting Information

The Supporting Information is available free of charge at https://pubs.acs.org/doi/10.1021/acscatal.2c03180.

Texture properties of EA-Co/SiO₂; comparison of the activity of EA-Co/SiO₂ with the literature; additional reactivity results of EA-Co/SiO₂ and IWI-Co/SiO₂ pretreated under various conditions; UV–vis characterization of EA-0.2Co/SiO₂ before and after high-temperature pretreatments; STEM images of EA-0.2Co/SiO₂-pretreated; IPA-TPD profile of EA-0.8Co/SiO₂ before and after high-temperature pretreatment; XPS and Raman characterizations; TPD profile of water; HRTEM of reduced and spent catalysts and IWI-Co/

SiO₂; EXAFS fitting details; and full FTIR spectra of 0.2Co/SiO₂-fresh (PDF)

AUTHOR INFORMATION

Corresponding Authors

Weiqing Zheng — RAPID Manufacturing Institute, Catalysis Center for Energy Innovation, Delaware Energy Institute, Center for Plastics Innovation, University of Delaware, Newark, Delaware 19716, United States; orcid.org/0000-0001-5854-4009; Email: weiqing@udel.edu

Dionisios G. Vlachos — Department of Chemical and Biomolecular Engineering, University of Delaware, Newark, Delaware 19716, United States; RAPID Manufacturing Institute, Catalysis Center for Energy Innovation, Delaware Energy Institute, Center for Plastics Innovation, University of Delaware, Newark, Delaware 19716, United States; orcid.org/0000-0002-6795-8403; Email: vlachos@udel.edu

Authors

Kewei Yu — Department of Chemical and Biomolecular Engineering, University of Delaware, Newark, Delaware 19716, United States; RAPID Manufacturing Institute, Catalysis Center for Energy Innovation, Delaware Energy Institute, Center for Plastics Innovation, University of Delaware, Newark, Delaware 19716, United States; orcid.org/0000-0002-8134-2541

Sanjana Srinivas — Department of Chemical and Biomolecular Engineering, University of Delaware, Newark, Delaware 19716, United States; RAPID Manufacturing Institute, Catalysis Center for Energy Innovation, Delaware Energy Institute, Center for Plastics Innovation, University of Delaware, Newark, Delaware 19716, United States

Cong Wang — RAPID Manufacturing Institute, Catalysis Center for Energy Innovation, Delaware Energy Institute, Center for Plastics Innovation, University of Delaware, Newark, Delaware 19716, United States; ◎ orcid.org/0000-0002-0451-344X

Weiqi Chen — RAPID Manufacturing Institute, Catalysis Center for Energy Innovation, Delaware Energy Institute, Center for Plastics Innovation, University of Delaware, Newark, Delaware 19716, United States

 Lu Ma – National Synchrotron Light Source, Brookhaven National Laboratory, Upton, New York 11973, United States
 Steven N. Ehrlich – National Synchrotron Light Source, Brookhaven National Laboratory, Upton, New York 11973, United States

- Nebojsa Marinkovic National Synchrotron Light Source, Brookhaven National Laboratory, Upton, New York 11973, United States
- Pawan Kumar Department of Materials Science and Engineering, University of Pennsylvania, Philadelphia, Pennsylvania 19104, United States; orcid.org/0000-0002-5764-2915
- Eric A. Stach Department of Materials Science and Engineering, University of Pennsylvania, Philadelphia, Pennsylvania 19104, United States; orcid.org/0000-0002-3366-2153
- Stavros Caratzoulas RAPID Manufacturing Institute, Catalysis Center for Energy Innovation, Delaware Energy Institute, Center for Plastics Innovation, University of Delaware, Newark, Delaware 19716, United States; orcid.org/0000-0001-9599-4199

Complete contact information is available at: https://pubs.acs.org/10.1021/acscatal.2c03180

Author Contributions

K.Y. performed the catalyst synthesis, FTIR, TPR, and XRD characterizations. K.Y. and W.C. carried out the reactivity tests. S.S. carried out the DFT calculations. K.Y. and C.W. conducted the TPD studies. L.M., S.E., and N.M. carried out the XAS measurements. P.K. and E.A.S. carried out the HAADF-STEM imaging. D.G.V., W.Z., and S.C. directed the project and provided guidance for the experimental and theoretical work. The manuscript was written by K.Y., W.Z., and D.G.V. with input from all authors.

Notes

The authors declare no competing financial interest.

ACKNOWLEDGMENTS

This work was supported by the Department of Energy's Office of Energy Efficient and Renewable Energy's Advanced Manufacturing Office under Award Number DE-EE0007888-8.3. The Delaware Energy Institute gratefully acknowledges the support and partnership of the State of Delaware toward the RAPID projects. XAS measurements were carried out at the 7-BM (QAS) beamline of the National Synchrotron Light Source II, a U.S. Department of Energy (DOE) Office of Science User Facility operated for the DOE Office of Science by Brookhaven National Laboratory under Contract No. DE-SC0012704. Additional resources at the 7-BM beamline were provided by the Synchrotron Catalysis Consortium, which was supported by the U.S. DOE, Office of Basic Energy Sciences, under grant no. DE-SC0012335. The authors acknowledge S.E., N.S.M., and L.M. for helping with the XAS measurements. XPS measurements were carried out using the Thermo Scientific K-Alpha+ XPS System at the University of Delaware surface analysis facility supported by NSF (no. 1428149). The authors acknowledge P.K. for the STEM imaging support; the work was carried out in part at the Singh Center for Nanotechnology, which was supported by the NSF National Nanotechnology Coordinated Infrastructure Program under grant NNCI-2025608. Additional support to the Nanoscale Characterization Facility at the Singh Center has been provided by the Laboratory for Research on the Structure of Matter (MRSEC) supported by the National Science Foundation (DMR-1720530).

REFERENCES

- (1) Sattler, J. J. H. B.; Ruiz-Martinez, J.; Santillan-Jimenez, E.; Weckhuysen, B. M. Catalytic Dehydrogenation of Light Alkanes on Metals and Metal Oxides. *Chem. Rev.* **2014**, *114*, 10613–10653.
- (2) Amghizar, I.; Vandewalle, L. A.; Van Geem, K. M.; Marin, G. B. New Trends in Olefin Production. *Engineering* **2017**, *3*, 171–178.
- (3) Nawaz, Z. Light Alkane Dehydrogenation to Light Olefin Technologies: A Comprehensive Review. *Rev. Chem. Eng.* **2015**, *31*, 413–436.
- (4) Bhasin, M. M.; McCain, J. H.; Vora, B. V.; Imai, T.; Pujadó, P. R. Dehydrogenation and Oxydehydrogenation of Paraffins to Olefins. *Appl. Catal., A* **2001**, *221*, 397–419.
- (5) Hu, B.; Schweitzer, N. M.; Zhang, G.; Kraft, S. J.; Childers, D. J.; Lanci, M. P.; Miller, J. T.; Hock, A. S. Isolated FeII on Silica As a Selective Propane Dehydrogenation Catalyst. *ACS Catal.* **2015**, *5*, 3494–3503.
- (6) Schweitzer, N. M.; Hu, B.; Das, U.; Kim, H.; Greeley, J.; Curtiss, L. A.; Stair, P. C.; Miller, J. T.; Hock, A. S. Propylene Hydrogenation and Propane Dehydrogenation by a Single-Site Zn2+ on Silica Catalyst. *ACS Catal.* **2014**, *4*, 1091–1098.
- (7) Camacho-Bunquin, J.; Aich, P.; Ferrandon, M.; "Bean" Getsoian, A.; Das, U.; Dogan, F.; Curtiss, L. A.; Miller, J. T.; Marshall, C. L.; Hock, A. S.; Stair, P. C. Single-Site Zinc on Silica Catalysts for Propylene Hydrogenation and Propane Dehydrogenation: Synthesis and Reactivity Evaluation Using an Integrated Atomic Layer Deposition-Catalysis Instrument. J. Catal. 2017, 345, 170–182.
- (8) Zhang, G.; Yang, C.; Miller, J. T. Tetrahedral Nickel(II) Phosphosilicate Single-Site Selective Propane Dehydrogenation Catalyst. *ChemCatChem* **2018**, *10*, 961–964.
- (9) Conley, M. P.; Delley, M. F.; Núñez-Zarur, F.; Comas-Vives, A.; Copéret, C. Heterolytic Activation of C–H Bonds on CrIII–O Surface Sites Is a Key Step in Catalytic Polymerization of Ethylene and Dehydrogenation of Propane. *Inorg. Chem.* **2015**, *54*, 5065–5078.
- (10) Cheng, Y.; Lei, T.; Miao, C.; Hua, W.; Yue, Y.; Gao, Z. Single-Site CrO_x Moieties on Silicalite: Highly Active and Stable for Ethane Dehydrogenation with CO2. *Catal. Lett.* **2018**, *148*, 1375–1382.
- (11) Koirala, R.; Buechel, R.; Pratsinis, S. E.; Baiker, A. Silica Is Preferred over Various Single and Mixed Oxides as Support for CO2-Assisted Cobalt-Catalyzed Oxidative Dehydrogenation of Ethane. *Appl. Catal., A* **2016**, 527, 96–108.
- (12) Koirala, R.; Safonova, O. V.; Pratsinis, S. E.; Baiker, A. Effect of Cobalt Loading on Structure and Catalytic Behavior of CoO_x/SiO2 in CO2-Assisted Dehydrogenation of Ethane. *Appl. Catal., A* **2018**, *552*, 77–85.
- (13) Estes, D. P.; Siddiqi, G.; Allouche, F.; Kovtunov, K. V.; Safonova, O. V.; Trigub, A. L.; Koptyug, I. V.; Copéret, C. C–H Activation on Co,O Sites: Isolated Surface Sites versus Molecular Analogs. J. Am. Chem. Soc. 2016, 138, 14987–14997.
- (14) Estes, D. P.; Cook, A. K.; Lam, E.; Wong, L.; Coperet, C. Understanding the Lewis Acidity of Co(II) Sites on a Silica Surface. *Inorg. Chem.* **2017**, *56*, 7731–7736.
- (15) Hu, B.; "Bean" Getsoian, A.; Schweitzer, N. M.; Das, U.; Kim, H.; Niklas, J.; Poluektov, O.; Curtiss, L. A.; Stair, P. C.; Miller, J. T.; Hock, A. S. Selective Propane Dehydrogenation with Single-Site CoII on SiO2 by a Non-Redox Mechanism. *J. Catal.* **2015**, 322, 24–37.
- (16) Zhao, Y.; Sohn, H.; Hu, B.; Niklas, J.; Poluektov, O. G.; Tian, J.; Delferro, M.; Hock, A. S. Zirconium Modification Promotes Catalytic Activity of a Single-Site Cobalt Heterogeneous Catalyst for Propane Dehydrogenation. *ACS Omega* **2018**, *3*, 11117–11127.
- (17) Huang, R.; Cheng, Y.; Ji, Y.; Gorte, R. J. Atomic Layer Deposition for Preparing Isolated Co Sites on SiO2 for Ethane Dehydrogenation Catalysis. *Nanomaterials* **2020**, *10*, No. 244.
- (18) Estes, D. P. Mechanistic Investigations of C–H Activations on Silica-Supported Co(Ii) Sites in Catalytic Propane Dehydrogenation. *Chimia* **2017**, *71*, No. 177.
- (19) Hu, B.; Kim, W.-G.; Sulmonetti, T. P.; Sarazen, M. L.; Tan, S.; So, J.; Liu, Y.; Dixit, R. S.; Nair, S.; Jones, C. W. A Mesoporous Cobalt Aluminate Spinel Catalyst for Nonoxidative Propane Dehydrogenation. *ChemCatChem* **2017**, *9*, 3330–3337.

- (20) Lee, S.; Halder, A.; Ferguson, G. A.; Seifert, S.; Winans, R. E.; Teschner, D.; Schlögl, R.; Papaefthimiou, V.; Greeley, J.; Curtiss, L. A.; Vajda, S. Subnanometer Cobalt Oxide Clusters as Selective Low Temperature Oxidative Dehydrogenation Catalysts. *Nat. Commun.* **2019**, *10*, No. 954.
- (21) Wang, Y.; Suo, Y.; Ren, J.-T.; Wang, Z.; Yuan, Z.-Y. Spatially Isolated Cobalt Oxide Sites Derived from MOFs for Direct Propane Dehydrogenation. *J. Colloid Interface Sci.* **2021**, *594*, 113–121.
- (22) Gao, Y.; Peng, L.; Long, J.; Wu, Y.; Dai, Y.; Yang, Y. Hydrogen Pre-Reduction Determined Co-Silica Interaction and Performance of Cobalt Catalysts for Propane Dehydrogenation. *Microporous Mesoporous Mater.* **2021**, 323, No. 111187.
- (23) Chen, C.; Zhang, S.; Wang, Z.; Yuan, Z.-Y. Ultrasmall Co Confined in the Silanols of Dealuminated Beta Zeolite: A Highly Active and Selective Catalyst for Direct Dehydrogenation of Propane to Propylene. *J. Catal.* **2020**, *383*, 77–87.
- (24) Bian, Z.; Dewangan, N.; Wang, Z.; Pati, S.; Xi, S.; Borgna, A.; Kus, H.; Kawi, S. Mesoporous-Silica-Stabilized Cobalt(II) Oxide Nanoclusters for Propane Dehydrogenation. ACS Appl. Nano Mater. 2021, 4, 1112–1125.
- (25) Li, X.; Wang, P.; Wang, H.; Li, C. Effects of the State of Co Species in Co/Al2O3 Catalysts on the Catalytic Performance of Propane Dehydrogenation. *Appl. Surf. Sci.* **2018**, 441, 688–693.
- (26) Sun, Y.; Wu, Y.; Shan, H.; Li, C. Studies on the Nature of Active Cobalt Species for the Production of Methane and Propylene in Catalytic Dehydrogenation of Propane. *Catal. Lett.* **2015**, *145*, 1413–1419.
- (27) Dewangan, N.; Ashok, J.; Sethia, M.; Das, S.; Pati, S.; Kus, H.; Kawi, S. Cobalt-Based Catalyst Supported on Different Morphologies of Alumina for Non-Oxidative Propane Dehydrogenation: Effect of Metal Support Interaction and Lewis Acidic Sites. *ChemCatChem* **2019**, *11*, 4923–4934.
- (28) Wu, L.; Ren, Z.; He, Y.; Yang, M.; Yu, Y.; Liu, Y.; Tan, L.; Tang, Y. Atomically Dispersed Co2+ Sites Incorporated into a Silicalite-1 Zeolite Framework as a High-Performance and Coking-Resistant Catalyst for Propane Nonoxidative Dehydrogenation to Propylene. ACS Appl. Mater. Interfaces 2021, 13, 48934–48948.
- (29) Hu, Z.-P.; Qin, G.; Han, J.; Zhang, W.; Wang, N.; Zheng, Y.; Jiang, Q.; Ji, T.; Yuan, Z.-Y.; Xiao, J.; Wei, Y.; Liu, Z. Atomic Insight into the Local Structure and Microenvironment of Isolated Co-Motifs in MFI Zeolite Frameworks for Propane Dehydrogenation. *J. Am. Chem. Soc.* **2022**, *144*, 12127–12137.
- (30) Wang, W.; Wu, Y.; Liu, T.; Zhao, Y.; Qu, Y.; Yang, R.; Xue, Z.; Wang, Z.; Zhou, F.; Long, J.; Yang, Z.; Han, X.; Lin, Y.; Chen, M.; Zheng, L.; Zhou, H.; Lin, X.; Wu, F.; Wang, H.; Yang, Y.; Li, Y.; Dai, Y.; Wu, Y. Single Co Sites in Ordered SiO2 Channels for Boosting Nonoxidative Propane Dehydrogenation. ACS Catal. 2022, 12, 2632—2638.
- (31) Guo, H.; Miao, C.; Hua, W.; Yue, Y.; Gao, Z. Cobaltous Oxide Supported on MFI Zeolite as an Efficient Ethane Dehydrogenation Catalyst. *Microporous Mesoporous Mater.* **2020**, No. 110791.
- (32) D'Souza, L.; Jiao, L.; Regalbuto, J. R.; Miller, J. T.; Kropf, A. J. Preparation of Silica- and Carbon-Supported Cobalt by Electrostatic Adsorption of Co(III) Hexaammines. *J. Catal.* **2007**, 248, 165–174.
- (33) Ravel, B.; Newville, M. ATHENA, ARTEMIS, HEPHAESTUS: Data Analysis for X-Ray Absorption Spectroscopy Using IFEFFIT. *J. Synchrotron Radiat.* **2005**, *12*, 537–541.
- (34) Frisch, M. J. GAUSSIAN09. https://gaussian.com/ (accessed June 29, 2022).
- (35) Becke, A. D. Density-Functional Thermochemistry. III. The Role of Exact Exchange. *J. Chem. Phys* **1993**, *98*, 5648–5652.
- (36) Grimme, S.; Antony, J.; Ehrlich, S.; Krieg, H. A Consistent and Accurate Ab Initio Parametrization of Density Functional Dispersion Correction (DFT-D) for the 94 Elements H–Pu. *J. Chem. Phys.* **2010**, 132, No. 154104.
- (37) Li, W.; Yu, S. Y.; Meitzner, G. D.; Iglesia, E. Structure and Properties of Cobalt-Exchanged H-ZSM5 Catalysts for Dehydrogenation and Dehydrocyclization of Alkanes. *J. Phys. Chem. B* **2001**, *105*, 1176–1184.

- (38) Jiao, L.; Regalbuto, J. R. The Synthesis of Highly Dispersed Noble and Base Metals on Silica via Strong Electrostatic Adsorption: I. Amorphous Silica. *J. Catal.* **2008**, *260*, 329–341.
- (39) Okamoto, Y.; Nagata, K.; Adachi, T.; Imanaka, T.; Inamura, K.; Takyu, T. Preparation and Characterization of Highly Dispersed Cobalt Oxide and Sulfide Catalysts Supported on Silica. *J. Phys. Chem.* A 1991, 95, 310–319.
- (40) Llusar, M.; Forés, A.; Badenes, J. A.; Calbo, J.; Tena, M. A.; Monrós, G. Colour Analysis of Some Cobalt-Based Blue Pigments. *J. Eur. Ceram. Soc.* **2001**, *21*, 1121–1130.
- (41) Reinen, D. Kationenverteilung Zweiwertiger 3d n-Ionen in Oxidischen Spinell-, Granat- und Anderen Strukturen. In *Structure and Bonding*; Springer: Berlin, Heidelberg, 1970; Vol. 7, pp 114–154.
- (42) Weakliem, H. A. Optical Spectra of Ni2+, Co2+, and Cu2+ in Tetrahedral Sites in Crystals. *J. Chem. Phys.* **1962**, *36*, 2117–2140.
- (43) Yu, S. Y.; Yu, G. J.; Li, W.; Iglesia, E. Kinetics and Reaction Pathways for Propane Dehydrogenation and Aromatization on Co/H-ZSM5 and H-ZSM5. *J. Phys. Chem. B* **2002**, *106*, 4714–4720.
- (44) Barzetti, T.; Selli, E.; Moscotti, D.; Forni, L. Pyridine and Ammonia as Probes for FTIR Analysis of Solid Acid Catalysts. *J. Chem. Soc., Faraday Trans.* **1996**, 92, 1401–1407.
- (45) Tamura, M.; Shimizu, K.; Satsuma, A. Comprehensive IR Study on Acid/Base Properties of Metal Oxides. *Appl. Catal., A* **2012**, 433–434, 135–145.
- (46) Pelmenschikov, A. G.; van Santen, R. A.; Janchen, J.; Meijer, E. Acetonitrile-D3 as a Probe of Lewis and Broensted Acidity of Zeolites. *J. Phys. Chem. B* **1993**, *97*, 11071–11074.
- (47) Platero, E. E.; Mentruit, M. P.; Morterra, C. Fourier Transform Infrared Spectroscopy Study of CD3CN Adsorbed on Pure and Doped γ -Alumina. *Langmuir* **1999**, *15*, 5079–5087.
- (48) Parry, E. An Infrared Study of Pyridine Adsorbed on Acidic Solids. Characterization of Surface Acidity. *J. Catal.* **1963**, *2*, 371–379.
- (49) Hemmann, F.; Agirrezabal-Telleria, I.; Jaeger, C.; Kemnitz, E. Quantification of Acidic Sites of Nanoscopic Hydroxylated Magnesium Fluorides by FTIR and 15 N MAS NMR Spectroscopy. *RSC Adv.* **2015**, *5*, 89659–89668.
- (50) McDonald, R. S. Surface Functionality of Amorphous Silica by Infrared Spectroscopy. J. Phys. Chem. C 1958, 62, 1168–1178.
- (51) Wang, C.; Mao, X.; Lee, J. D.; Onn, T. M.; Yeh, Y.-H.; Murray, C. B.; Gorte, R. J. A Characterization Study of Reactive Sites in ALD-Synthesized WOx/ZrO2 Catalysts. *Catalysts* **2018**, *8*, No. 292.
- (52) Kostestkyy, P.; Yu, J.; Gorte, R. J.; Mpourmpakis, G. Structure—Activity Relationships on Metal-Oxides: Alcohol Dehydration. *Catal. Sci. Technol.* **2014**, *4*, 3861–3869.